Supplementary information

Simplified simulation of rock avalanches and subsequent debris flows with a single thin-layer model. Application to the Prêcheur river (Martinique, Lesser Antilles)

Marc Peruzzetto[1, 2], Clara Levy[2], Yannick Thiery[2], Gilles Grandjean[2], Anne Mangeney[1], Anne-Marie Lejeune[1,3], Aude Nachbaur[4], Yoann Legendre[5], Benoit Vittecoq[4], Jean-Marie Saurel[1], Valérie Clouard[6], Thomas Dewez[2], Fabrice Fontaine[1,3], Martin Mergili[7], Sophie Lagarde[1,8], Jean-Christophe Komorowski[1], Anne Le Friant[1], and Arnaud Lemarchand[1]

[1] Université de Paris, Institut de physique du globe de Paris, CNRS, F-75005 Paris, France

[2]BRGM, Orléans, France

[3]Observatoire volcanologique et sismologique de la Martinique, Institut de physique du globe de Paris, F-97250 Fonds Saint Denis, France.

[4]BRGM Martinique, 7200 Fort-de-France, France

[5]BRGM Guadeloupe, 97170 Petit-Bourg, France

[6]GET/OMP - UMR 5563 CNRS - UM 97 UPS - UR 234 IRD - CNES, Toulouse, France

[7]Institute of Geography and Regional Science, University of Graz, Graz, Austria

[8]Section 4.6 Geomorphology, GFZ German Research Centre for Geosciences, Postdam, Germany

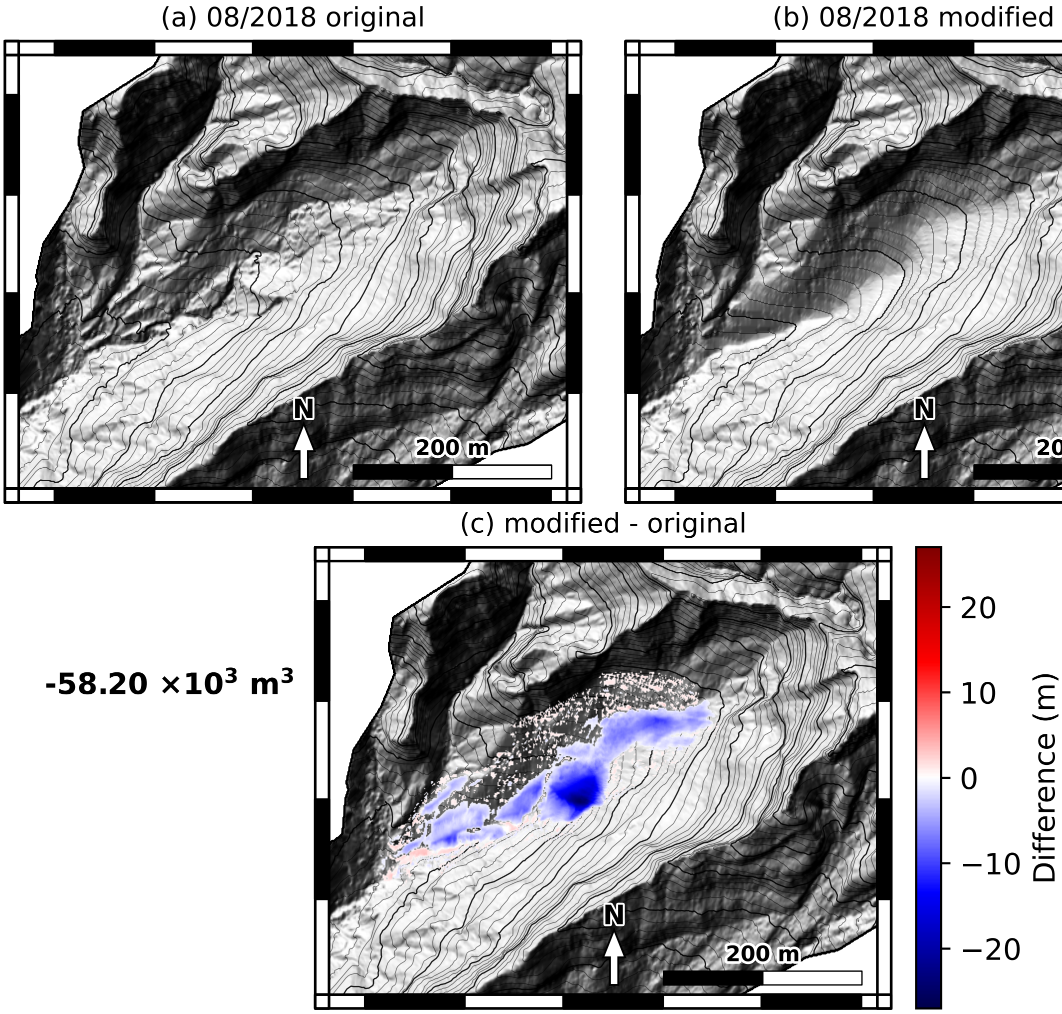

Supplementary Figure 1: Modification of the 08/2018 DEM to remove screes at the bottom of the cliff. (a) Original 08/2018 DEM. (b) Modified 08/2018 DEM, without screes). (c) Difference between modified and original DEM. We give the volume corresponding to the screes removed. Bold contour interval is 50 m, thin contour interval is 10 m.

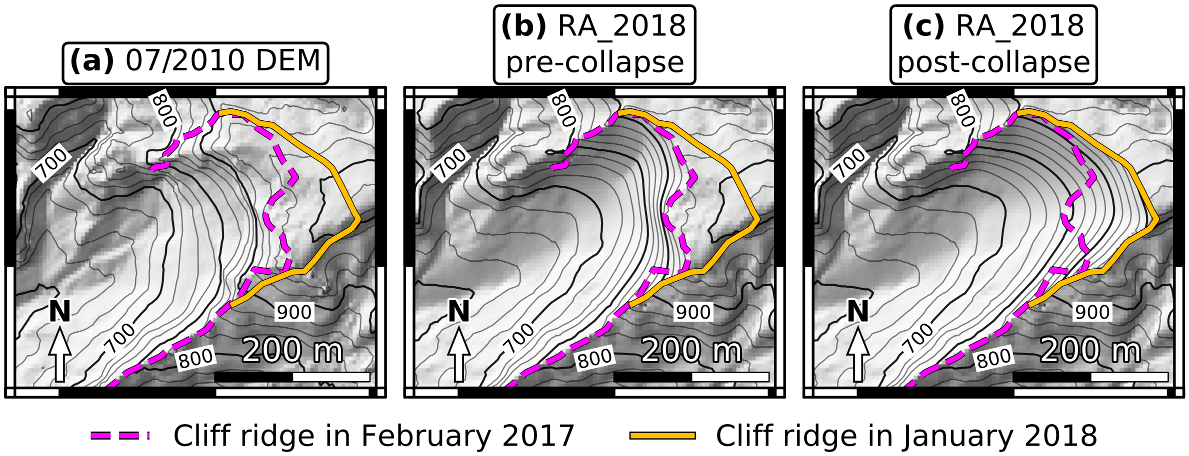

Supplementary Figure 2: Reconstruction of the pre 2018 collapse cliff geometry for *RA_ 2018* scenario. (a) Cliff in July 2010. (b) Synthetic reconstruction of the cliff topography based on the 2017 cliff rim (top of *RA_ 2018* unstable volume). (c) Cliff on Jan. 19, 2018 modified to remove deposits at the cliff bottom.

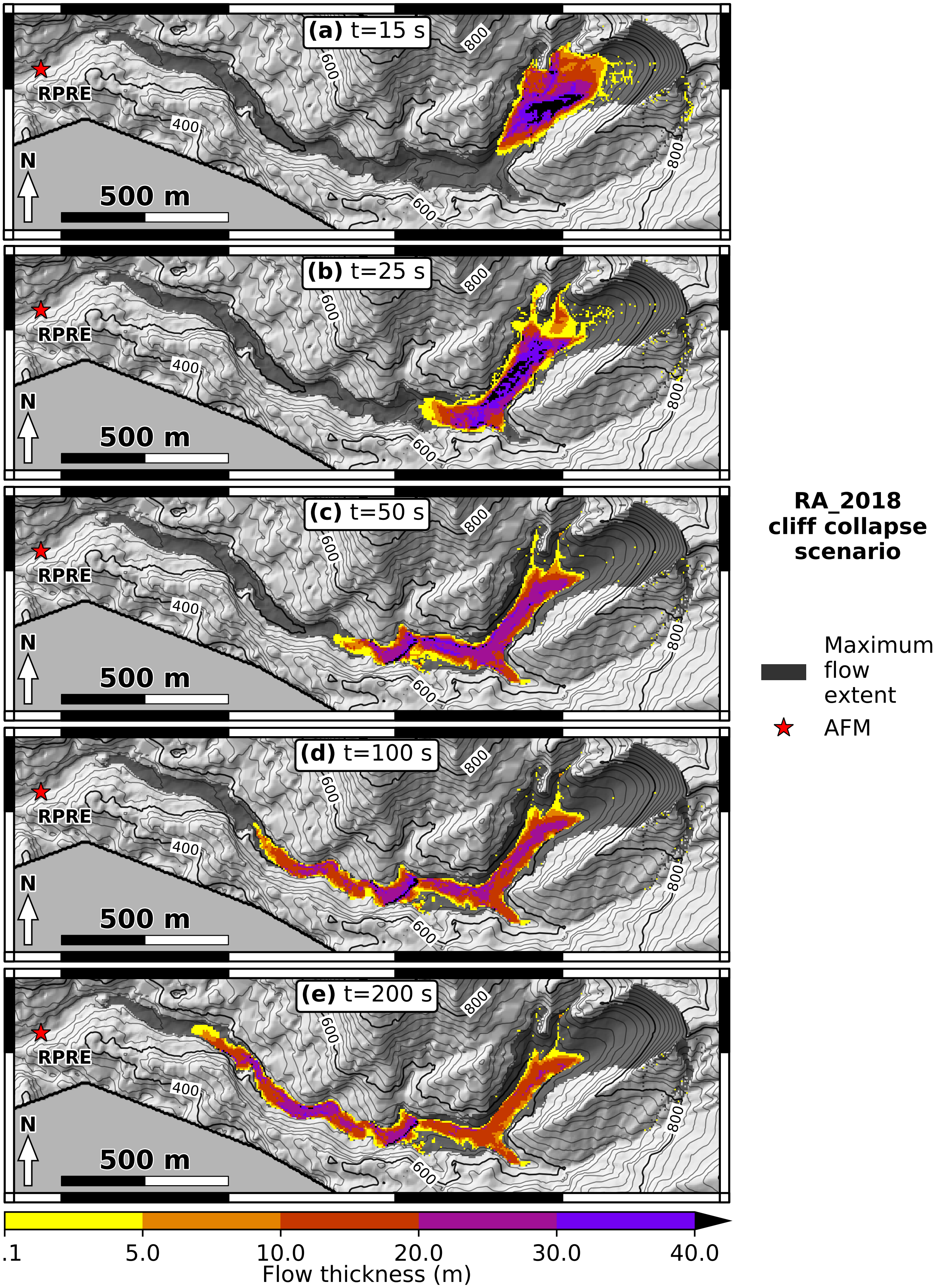

Supplementary Figure 3: *RA_2018* simulation with Coulomb rheology and $\mu_S = \tan(14°) = 0.25$. Flow thickness is given at (a) $t = 15$ s, (b) $t = 25$ s, (c) $t = 50$ s, (d) $t = 100$ s and (e) $t = 200$ s.

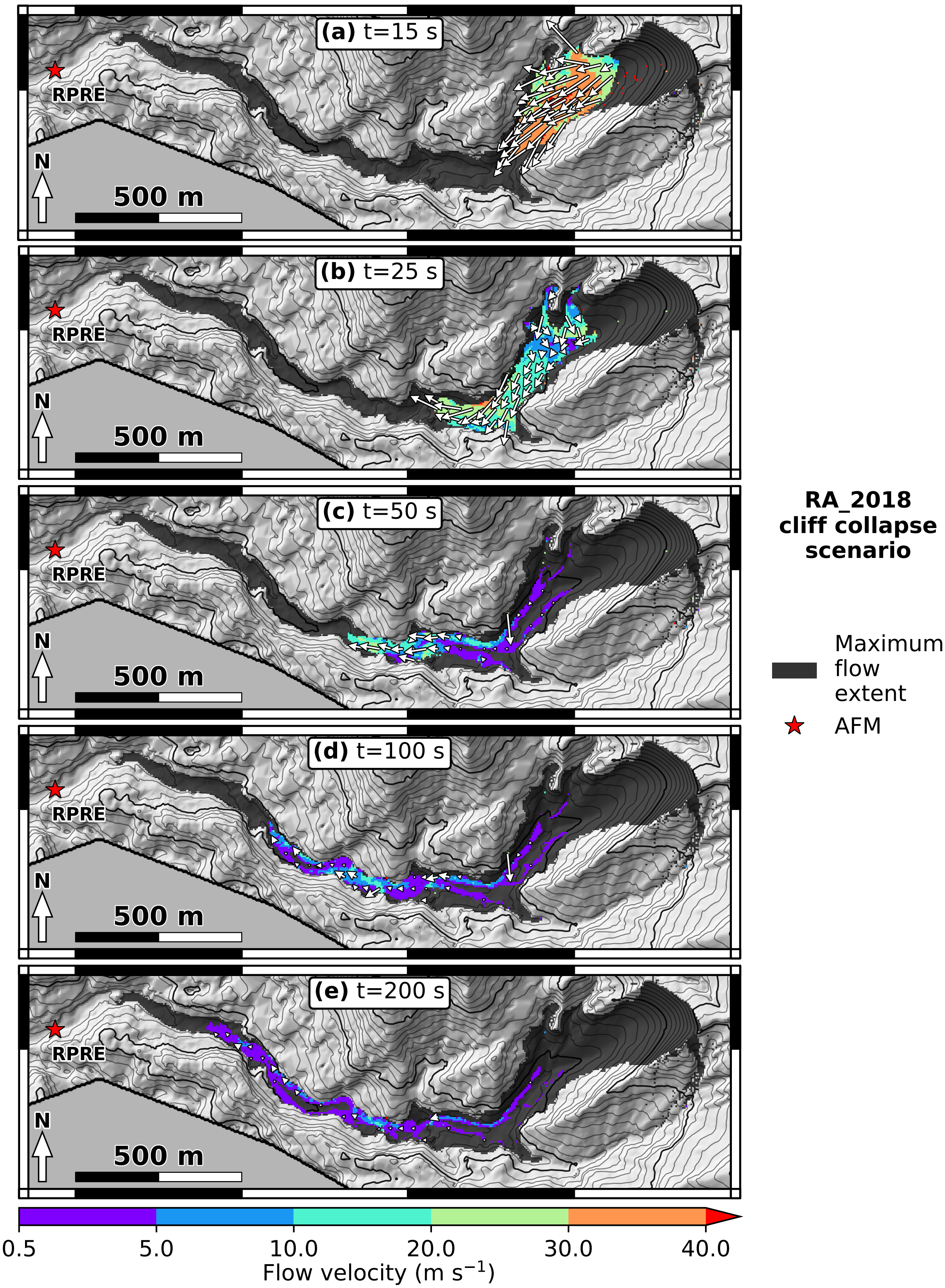

Supplementary Figure 4: *RA_2018* simulation with Coulomb rheology and $\mu_S = \tan(14°) = 0.25$. Flow velocity is given at (a) $t = 15$ s, (b) $t = 25$ s, (c) $t = 50$ s, (d) $t = 100$ s and (e) $t = 200$ s. Small white arrows give flow velocity direction.

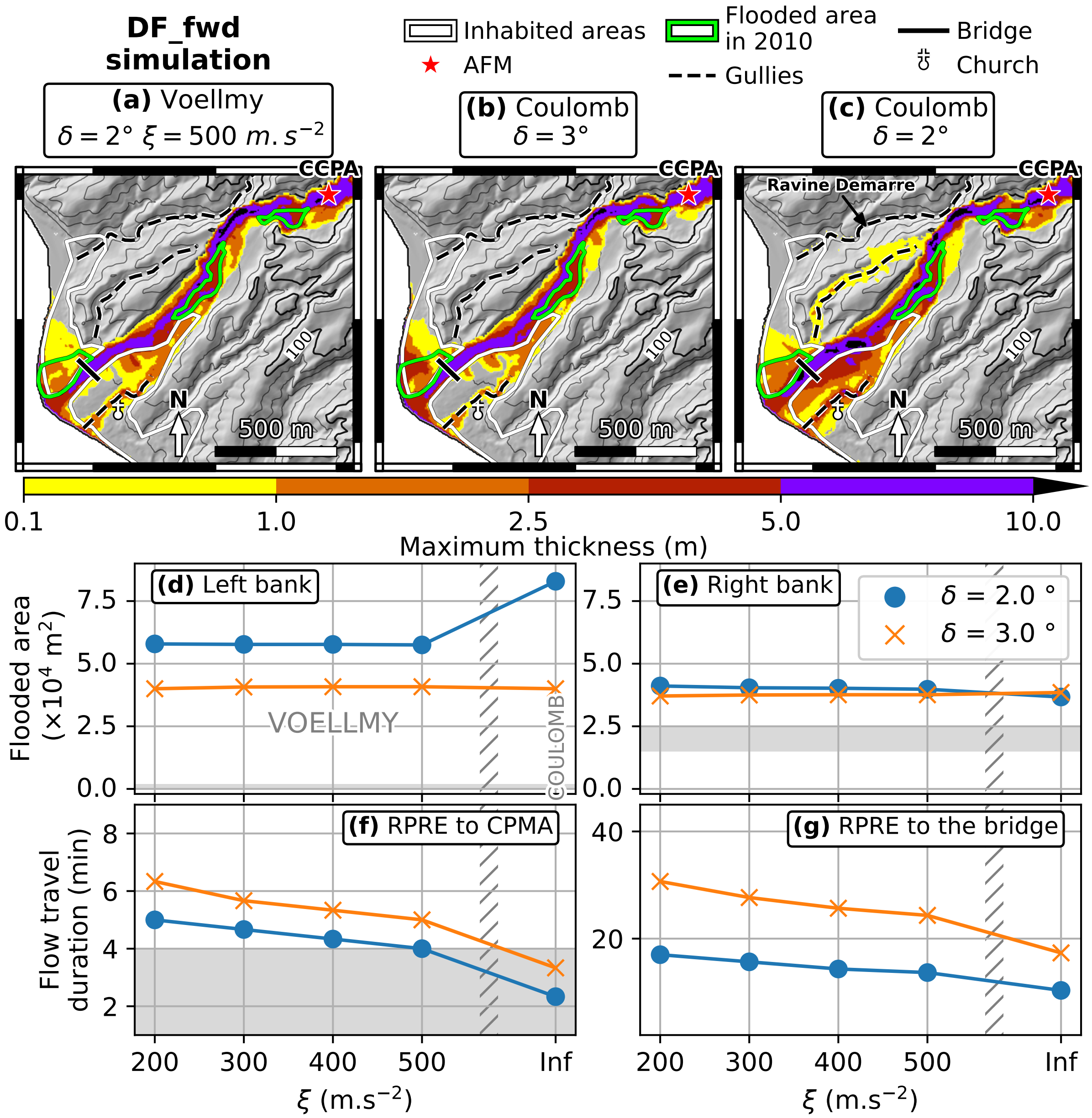

Supplementary Figure 5: Simulation results for the *DF_fwd* scenario. (a) Maximum flow thickness with the Voellmy rheology, $\mu_S = \tan(2°) = 0.03$ and $\xi = 500$ m s^{-2}. (b) Maximum flow thickness with the Coulomb rheology and $\mu_S = \tan(3°) = 0.05$. (c) Maximum flow thickness with the Coulomb rheology and $\mu_S = \tan(2°) = 0.03$. Topography is represented by the 08/2018 DEM. Each point in (d), (e), (f) and (g) is a simulation result, with friction coefficient given by line color and turbulence coefficients given by the x-coordinate. Left of hatches is for the Voellmy rheolgy, right is for the Coulomb rheology (equivalent to infinite turbulence coefficient). (d) Flow travel duration between RPRE and CPMA (about 1.6 km). They are measured by picking the maximum of the discharge at each location. (e) Flow travel duration between RPRE and the Prêcheur bridge (about 4.3 km). (f) Area flooded on the left river bank, within inhabited areas. (g) Area flooded on the right river bank, within inhabited areas. Grey patches give observations ranges for the Jun. 19, 2010 DF.

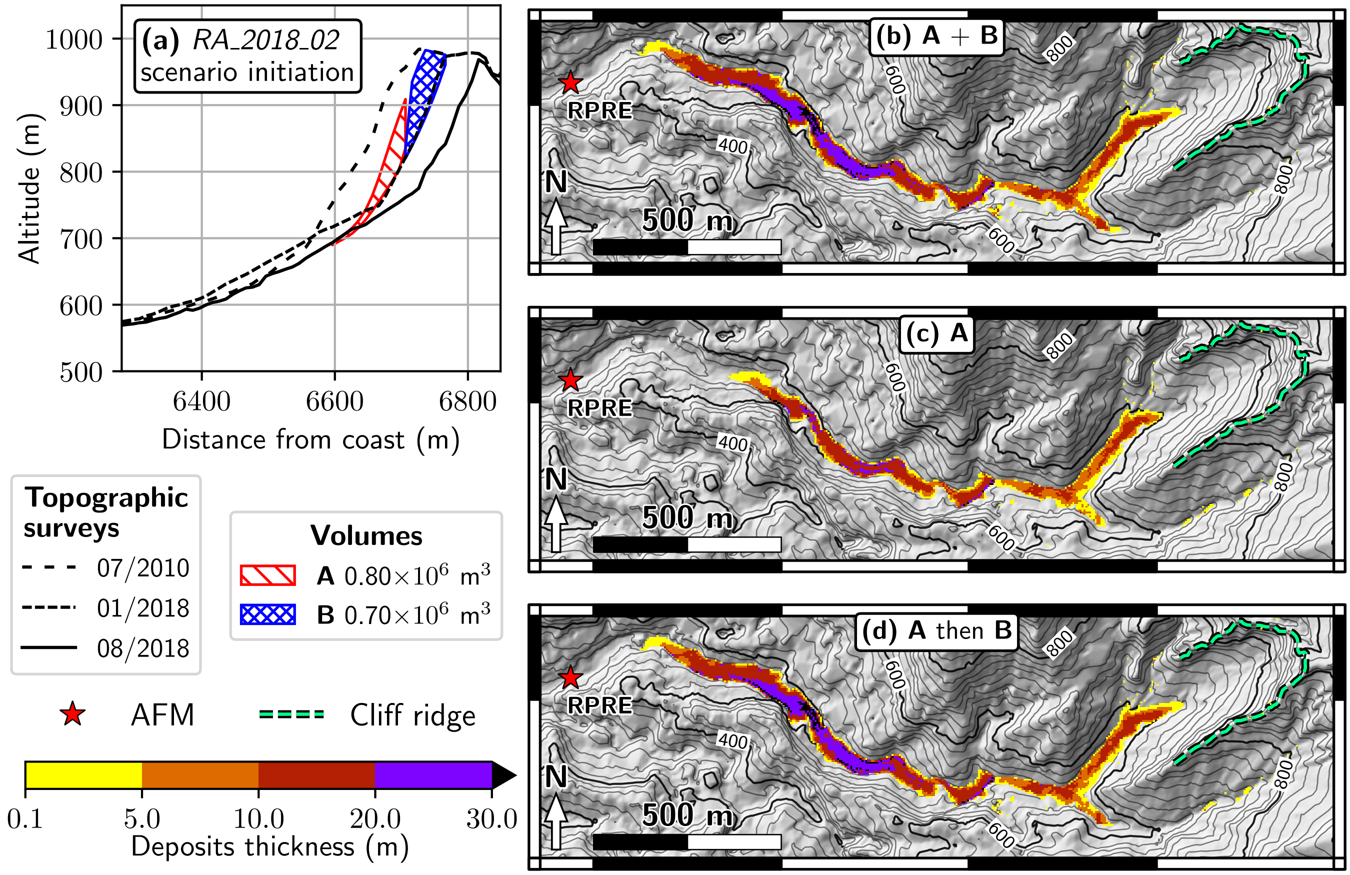

Supplementary Figure 6: *RA_ 2018_ 2* scenario, with two successive collapses. (a) Black lines: topographic surveys. Red hatched patch (A): first initial 0.8×10^6 m^3 collapse. Blue hatched patch (B): second 0.7×10^6 m^3 collapse, 13 s after initiation. (b) Final deposits of *RA_ 2018* scenario, with A and B collapsing at once. (c) Final deposits when only A collapses. (d) Final deposits of the *sc_ 2018_ 2* scenario, with A collapsing, followed by B 13 s later. All simulations are done with the Coulomb rheology and $\mu_S = \tan(14°) = 0.25$. Green dashed line: Samperre cliff rim. Topography in (b), (c) and (d) is the 08/2018 DEM.

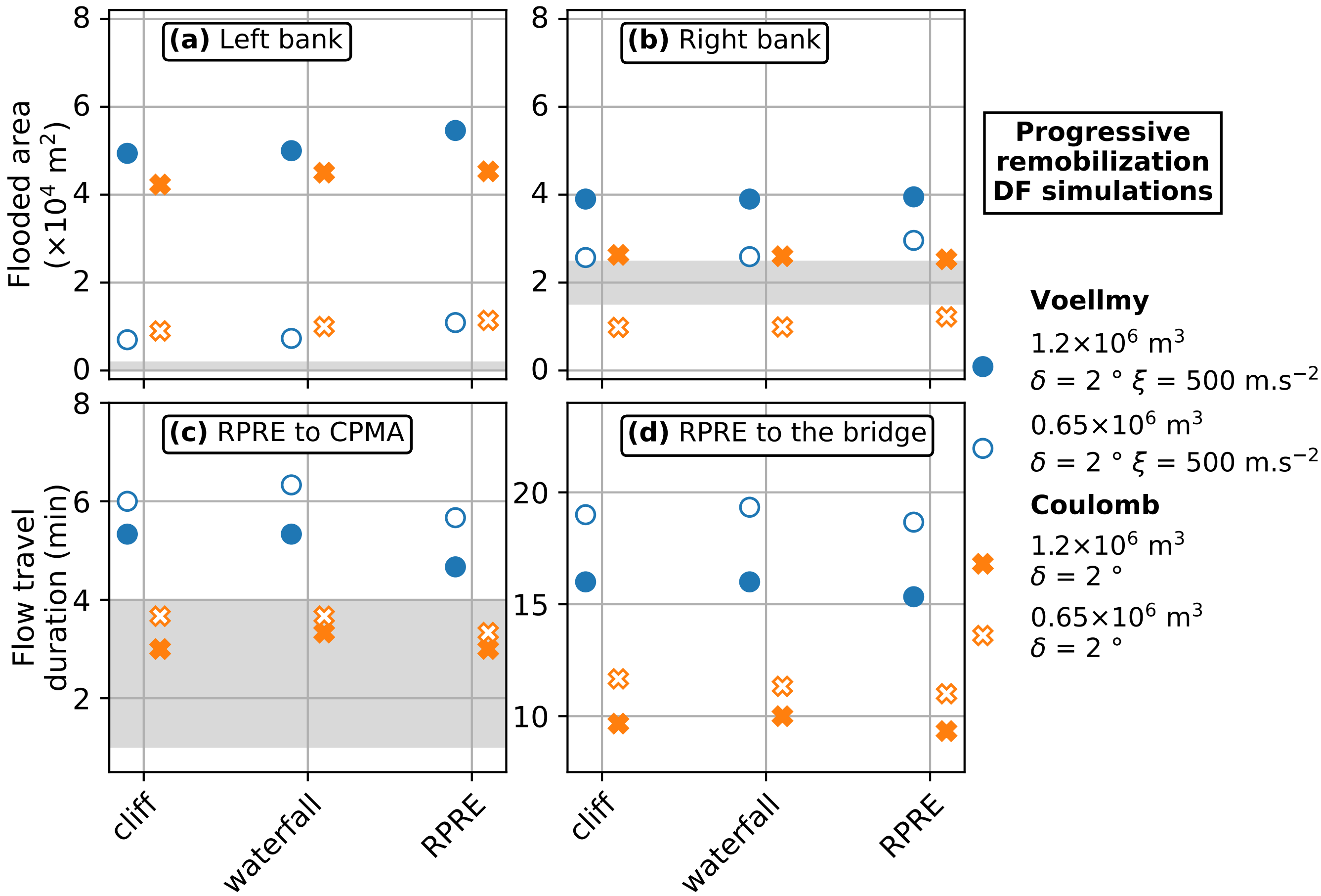

Supplementary Figure 7: Results of DF simulations with 1.2×10^6 m^3 (filled markers) and 0.65×10^6 m^3 (empty markers), with a constant source discharge imposed during 10 min, at different locations (see abcissa). (a) Area flooded in the Precheur village, left bank. (b) Area flooded in the Prêcheur village, right bank. (c) Travel durations between RPRE and CPMA. (d) Travel durations between RPRE and the bridge. Durations refer to discharge onsets. Grey patches are observations for the Jun. 19, 2010 DF.

Supplementary Table 1: Data used to plot Figure 12 in the main body of the article, giving the calibrated friction angles δ and corresponding friction coefficients $\mu_S = \tan(\delta)$ derived for different sites with the SHALTOP numerical model. Values in bold are found in the specified references, from which we deduce the corresponding value for δ or μ_S.

Reference	Site	Volume (m^3)	δ (°)	$\mu_S = \tan(\delta)$	Calibration data
(Lucas et al., 2007)	Shum Wam	2.60×10^4	**18**	0.32	deposits
	Fei Tsui	1.40×10^4	**26**	0.49	deposits
	Frank Slide	3.60×10^7	**12**	0.21	deposits
(Peruzzetto et al., 2019)	Soufriere (1530 CE)	9.30×10^7	**7**	0.12	deposits
(Yamada et al., 2018)	Akatani	7.38×10^6	16.7	**0.3**	seismic signal
	Iya	4.67×10^6	17.7	**0.32**	seismic signal
	Nagatono	3.63×10^6	21.8	**0.4**	seismic signal
	Nonoo	2.72×10^6	19.8	**0.36**	seismic signal
(Moretti et al., 2015)	Mount Meager	4.85×10^7	18.3	**0.33**	seismic signal + deposits
(Moretti et al., 2020)	Montserrat (1997 CE)	4.58×10^7	**14.2**	0.25	seismic signal
(Kuo et al., 2009)	Tsaoling, Taiwan	1.50×10^8	**6**	0.11	deposits

Supplementary Note 1: Seismic energy and simulated dissipiated energy

Following Schneider et al. (2010) and Levy et al. (2015), we compare the dissipated energy rate P_{SH} during the simulation to the seismic energy rate P_s. This allows to see if the simulated duration of of the rock avalanche is similar to the duration of the generated signal, which is a good proxy for the actual duration of the rock avalanche (Levy et al., 2015). Temporal variations of P_{SH} and P_s can also help characterizing the dynamics of the rock avalanche, and in particular determining if the initial collapse happened in one or several successive steps. We define P_{SH} as:

$$P_{SH} = -\frac{d}{dt}\left(E_k + E_p\right), \tag{1}$$

with E_k the total flow kinetic energy and E_p the total flow potential energy. This is equivalent to computing the energy dissipated by the basal friction force. P_S is computed with the 0.1-20 Hz filtered seismic signal recorded at the LAM station, about 1300 m away from the cliff. Following Vilajosana et al. (2008), Levy et al. (2015) and Durand et al. (2018), the seismic energy E_S is:

$$E_S = 2\pi r \rho h c e^{\alpha r} \int_{t=t_{init}}^{t=t_{final}} \left(u_E^2 + u_N^2 + u_Z^2\right) dt, \tag{2}$$

where u_E, u_N and u_Z are respectively the eastern, northern and vertical components of the seismic recording (deconvolved from the instrumental response), and where we assumed a point-source and an isotropic and homogeneous medium. We also consider that seismic surface waves dominate the signal. The parameters are $r = 1300$ m the distance to the signal source, $\rho = 2000$ kg m^{-3} the density of the materials in which waves propagate, h m the thickness of the layer in which waves propagate, c the group seismic wave velocity, and α an attenuation parameter.

α, h and c are frequency dependent. Besides, much more complex topographic corrections should be needed in (2) (Kuehnert et al., 2020). However, Levy et al. (2015) find no major difference between the energy integrated over successive frequency bands and the energy computed directly as in (2), when the frequency band includes the frequencies concentrating most of the energy (in our case, around 2 Hz). Furthermore, we are more interested in trends than absolute values. Thus, we simply define P_S as

$$P_S = \frac{dEs}{dt} = 2\pi r \rho h c e^{\alpha r} \left(u_E^2 + u_N^2 + u_Z^2 \right). \tag{3}$$

We assume a surface wave velocity $c = 1300$ m s^{-1} as in Levy et al. (2015). Considering that most of the energy of the signal is at $f = 2$ Hz, we follow Levy et al. (2015) and get:

$$h = 2.5 \frac{c}{f} = 1625 \text{ m} \tag{4}$$

$$\alpha = 2.4 \times 10^{-4} f^{0.4} = 3.1 \times 10^{-4} \text{ m}^{-1} \tag{5}$$

Lowess smoothing (Seabold and Perktold, 2010) is applied to the resulting time series. Note that the constants above only act as scaling factors but do not change temporal variations of P_S.

References

Durand, V., Mangeney, A., Haas, F., Jia, X., Bonilla, F., Peltier, A., Hibert, C., Ferrazzini, V., Kowalski, P., Lauret, F., Brunet, C., Satriano, C., Wegner, K., Delorme, A., and Villeneuve, N. (2018). On the Link Between External Forcings and Slope Instabilities in the Piton de la Fournaise Summit Crater, Reunion Island. *Journal of Geophysical Research: Earth Surface*, 123(10):2422–2442.

Kuehnert, J., Mangeney, A., Capdeville, Y., Métaxian, J. P., Bonilla, L. F., Stutzmann, E., Chaljub, E., Boissier, P., Brunet, C., Kowalski, P., Lauret, F., and Hibert, C. (2020). Simulation of Topography Effects on Rockfall-Generated Seismic Signals: Application to Piton de la Fournaise Volcano. *Journal of Geophysical Research: Solid Earth*, 125(10):e2020JB019874.

Kuo, C. Y., Tai, Y. C., Bouchut, F., Mangeney, A., Pelanti, M., Chen, R. F., and Chang, K. J. (2009). Simulation of Tsaoling landslide, Taiwan, based on Saint Venant equations over general topography. *Engineering Geology*, 104(3):181–189.

Levy, C., Mangeney, A., Bonilla, F., Hibert, C., Calder, E. S., and Smith, P. J. (2015). Friction weakening in granular flows deduced from seismic records at the Soufrière Hills Volcano, Montserrat. *Journal of Geophysical Research: Solid Earth*, 120(11):7536–7557.

Lucas, A., Mangeney, A., Bouchut, F., Bristeau, M.-O., and Mège, D. (2007). Benchmarking Exercises for Granual Flows. In *The 2007 International Forum on Landslide Disaster Management*, Hong Kong. Ho & Li.

Moretti, L., Allstadt, K., Mangeney, A., Capdeville, Y., Stutzmann, E., and Bouchut, F. (2015). Numerical modeling of the Mount Meager landslide constrained by its force history derived from seismic data. *Journal of Geophysical Research: Solid Earth*, 120(4):2579–2599.

Moretti, L., Mangeney, A., Walter, F., Capdeville, Y., Bodin, T., Stutzmann, E., and Le Friant, A. (2020). Constraining landslide characteristics with Bayesian inversion of field and seismic data. *Geophysical Journal International*, 221(2):1341–1348.

Peruzzetto, M., Komorowski, J.-C., Friant, A. L., Rosas-Carbajal, M., Mangeney, A., and Legendre, Y. (2019). Modeling of partial dome collapse of La Soufrière of Guadeloupe volcano: Implications for hazard assessment and monitoring. *Scientific Reports*, 9(1):1–15.

Schneider, D., Bartelt, P., Caplan-Auerbach, J., Christen, M., Huggel, C., and McArdell, B. W. (2010). Insights into rock-ice avalanche dynamics by combined analysis of seismic recordings and a numerical avalanche model. *Journal of Geophysical Research*, 115(F4).

Seabold, S. and Perktold, J. (2010). Statsmodels: Econometric and statistical modeling with python. In *Proceedings of the 9th Python in Science Conference*.

Vilajosana, I., Suriñach, E., Abellán, A., Khazaradze, G., Garcia, D., and Llosa, J. (2008). Rockfall induced seismic signals: Case study in Montserrat, Catalonia. *Natural Hazards and Earth System Sciences*, 8(4):805–812.

Yamada, M., Mangeney, A., Matsushi, Y., and Matsuzawa, T. (2018). Estimation of dynamic friction and movement history of large landslides. *Landslides*, 15(10):1963–1974.